

Concerted Metal Cation Desorption and Proton Transfer on Deprotonated Silica Surfaces

Kevin Leung*, Louise J. Criscenti, Andrew W. Knight,
Anastasia G. Ilgen, Tuan A. Ho, and Jeffery A. Greathouse

Sandia National Laboratories, MS 1415,

8 0754, Albuquerque, NM 87185

*kleung@sandia.gov

(Dated: November 2, 2018)

Abstract

The adsorption equilibrium constants of monovalent and divalent cations to material surfaces in aqueous media are central to many technological, natural, and geochemical processes. Cation adsorption/desorption is often proposed to occur in concert with proton-transfer on hydroxyl-covered mineral surfaces, but so far this cooperative effect has been inferred indirectly. This work applies Density Functional Theory (DFT)-based molecular dynamics simulations of explicit liquid water/mineral interfaces to calculate metal ion desorption free energies. Monodentate adsorption of Na^+ , Mg^{2+} , and Cu^{2+} on partially deprotonated silica surfaces are considered. Na^+ is predicted to be unbound, while Cu^{2+} exhibits larger binding free energies to surface SiO^- groups than Mg^{2+} . The predicted trends agree with competitive adsorption measurements on fumed silica surfaces. As desorption proceeds, Cu^{2+} dissociates one of the H_2O molecules in its first solvation shell, turning into $\text{Cu}^{2+}(\text{OH}^-)(\text{H}_2\text{O})_3$, while Mg remains $\text{Mg}^{2+}(\text{H}_2\text{O})_6$. The protonation state of the SiO^- group at the initial binding site does not vary monotonically with cation desorption.

The adsorption free energies of ions on to material surfaces in liquid media govern equilibrium constants and adsorption isotherms, which are central to many technological and geochemical processes.¹⁻⁵ One key aspect of interfaces between aqueous electrolyte and materials interface, distinct from those of aprotic solvents, is the possibility of acid-base reactions occurring in conjunction with ion adsorption. Surface hydroxyl (-OH) groups, ubiquitous at water interfaces, can release H^+ as cations adsorb, especially for multivalent cations. OH^- can also be released as oxyanions bind to the surface.⁴ This phenomenon is well known in geochemistry contexts,⁶⁻⁸ but its occurrence is generally inferred indirectly from measurements or estimated from continuum models. Computationally, it has been shown that divalent cation binding energies at water-oxide interface can differ by a very large amount – ~ 2 eV (46 kcal/mol)⁹ – depending on whether surface OH groups are deprotonated or not. But the computational method used there, and in most existing molecular calculations, does not permit spontaneous, simultaneous deprotonation and cation adsorption events. It begs the question of what quantitative effect allowing such cooperative behavior would make. Benchmark calculations are urgently needed.

Apart from this cooperativity, understanding many aspects of cation adsorption remains challenging. Tremendous progress has been made via non-linear optical spectroscopy,⁸ nuclear magnetic resonance (NMR),¹⁰ X-ray photoelectron spectroscopy and other X-ray methods,^{4,11,12} titration,¹³ batch adsorption,^{14,15} and calorimetry techniques¹⁶ to investigate cation adsorption, including on silica surfaces which are ubiquitous in many applications and areas of science. But disagreements about fundamental aspects, such as whether cations are adsorbed in outer-^{8,10} or inner-sphere¹⁶ configurations, have persisted. Here inner-sphere means direct contact between SiO^-/M^+ , while outer-sphere is water-mediated adsorption, $SiO^-/H_2O/M^+$.

Atomic length-scale modeling can shed light on many aspects of cation adsorption.^{9,17-20} In particular, force field-based potential-of-mean-force (PMF) calculations have been successfully applied to study divalent metal cations desorption from mineral surfaces.^{9,18} However, it is challenging to use non-electronic structure methods to model the interactions between transition metal (TM) cations and ligands.⁷ This is because TM ions with partially filled $3d$ orbitals are difficult to parameterize with molecular force fields. Furthermore, with few exceptions,²¹⁻²³ most existing force fields for minerals do not permit dynamical changes in the protonation states in the ubiquitous hydroxyl groups on mineral surfaces. Molecular

dynamics studies have generally resorted to static assignment of surface hydroxyl deprotonation states. This approach cannot address correlations and dynamical fluctuations in the electrostatic environments of binding sites due to acid-base reactions.

The present work highlights the coupled cation desorption/material surface proton transfer phenomenon, using Density Functional Theory (DFT)-based molecular dynamics (or “*ab initio* molecular dynamics”/AIMD) simulations. AIMD has been shown to predict acid-base reactions to within 1 pH unit.^{24–35} DFT also explicitly includes the effect of partial *3d* orbital occupancies. AIMD is therefore well-suited to modeling metal adsorption on mineral surfaces with OH groups at binding sites.^{7,28,36,37} Existing AIMD work have not directly addressed cooperative acid-base/cation adsorption, partly because some materials surfaces previously examined may not exhibit this behavior and partly because PMF methods have not been applied to pull cations sufficiently far from the surface. Our AIMD results will be supported by batch adsorption isotherm experiments and compared with classical force field predictions.

The cations of interest here are Na^+ , Mg^{2+} , and Cu^{2+} . The model substrate chosen is a reconstructed β -crystabellite (001) surface, with about $4/\text{nm}^2$ SiOH group surface density.³³ It has several advantages as a benchmark. (1) The surface SiOH density is in reasonable accord with that cited for well-soaked, amorphous silica.³⁸ (2) We have previously computed its pK_a using AIMD potential-of-mean-force calculations, and can therefore correlate this pK_a with cation desorption calculations conducted using similar AIMD methods. (3) The surface has a moderate cell size, and only one distinct type of silanol (SiOH) group. Each SiOH is at least 5 \AA from all other SiOH, ensuring that cations can only coordinate to one SiO^- group on this model surface (i.e., they are monodentate). This feature simplifies the computational analysis. In contrast, many crystalline mineral surfaces feature numerous cation-binding sites and types of hydroxyl groups.⁷

Finite temperature AIMD simulations apply the Perdew-Burke-Ernzerhof (PBE) functional,³⁹ the projector-augmented wave-based Vienna Atomic Simulation Package (VASP),^{40,41} a 400 eV energy cutoff, and Γ -point sampling of the Brillouin zone. All simulation cells have dimensions $10.12 \text{ \AA} \times 10.12 \text{ \AA} \times 26.0 \text{ \AA}$. These settings are similar to those in our previous pK_a work.^{33,34} Spin-polarized DFT calculations, with one net unpaired electron, are conducted when Cu^{2+} is present. The Cu pseudopotential used does not include pseudovalent *3p* electrons. To keep the simulation cells charge neutral, one or two H^+ are removed

from the silica surface with an adsorbed cation. One of the resulting SiO^- is initially coordinated to the M^{n+} . The overall stoichiometries are $\text{Si}_{20}\text{O}_{107}\text{H}_{133}^-\text{Na}^+$ and $\text{Si}_{20}\text{O}_{108}\text{H}_{134}^-\text{M}^{2+}$. For details of the initiation of AIMD simulation cells, see the Supporting Information (S.I.) document.

In the presence of acid functional groups at water/material interfaces, the pH in the simulation cell should be pinned at the pK_a of functional groups, provided that (1) there is only one type of such groups; (2) a fraction of them are deprotonated; (3) their pK_a is lower than that of H_2O ; and (4) the surface groups do not interact with each other. Within the non-interacting assumption, the pH in our AIMD cells should be between 7.0 and 8.1 – the pK_a range previously predicted for this surface.³³ In experimental samples with amorphous or crystalline silica, bimodal or trimodal pK_a distributions of pK_a have been reported.^{42,43} It would have been more challenging to assign pK_a in AIMD simulation cells with multiple types of SiOH .

Potential-of-mean-force (PMF) free energy simulations computes $\Delta W(Z)$ as the natural logarithm of the probability distribution of the two-body reaction coordinate of the form $Z=z_{\text{O}} - z_{\text{M}}$ (S.I.). Here Z is the coordinate normal to the silica-water interface, M is the desorbing cation, and O is part of the initially deprotonated surface SiOH group bound to M^{n+} . The first window represents configurations with M^{n+} bound to the SiO^- group; subsequent windows have M^{n+} progressively displaced farther away.

$\Delta W(Z)$ is effectively the constrained free energy at a Z value; it includes neither fluctuations around Z nor the standard state reference associated with aqueous solutions. To obtain the adsorption free energy (ΔG_{ads}) from $\Delta W(Z)$, we integrate configuration space in three dimensions, and account for the entropic contribution from a standard state 1.0 M ideal concentration solution:⁴⁴

$$\Delta G_{\text{ads}}/k_{\text{B}}T = -\log\left\{\int_{\Omega} d\Omega \exp[-\Delta W(Z)/k_{\text{B}}T]/(V_o)\right\}. \quad (1)$$

Here V_o is the volume associated with 1.0 M aqueous solution (1662 \AA^3) and $T=300 \text{ K}$ is assumed. The volume element Ω spans the configuration space where M^{n+} is “bonded” to the SiO^- group. A limiting bonding distance of 2.50 \AA is assumed. At this separation the pair correlation functions between transition metal ions and water oxygen sites exhibits their first turning points.⁴⁵ The angular distribution is also involved in the integral. To our knowledge, Ω has not been standardized for PMF calculations at interfaces.^{9,18,37} Here we approximate it

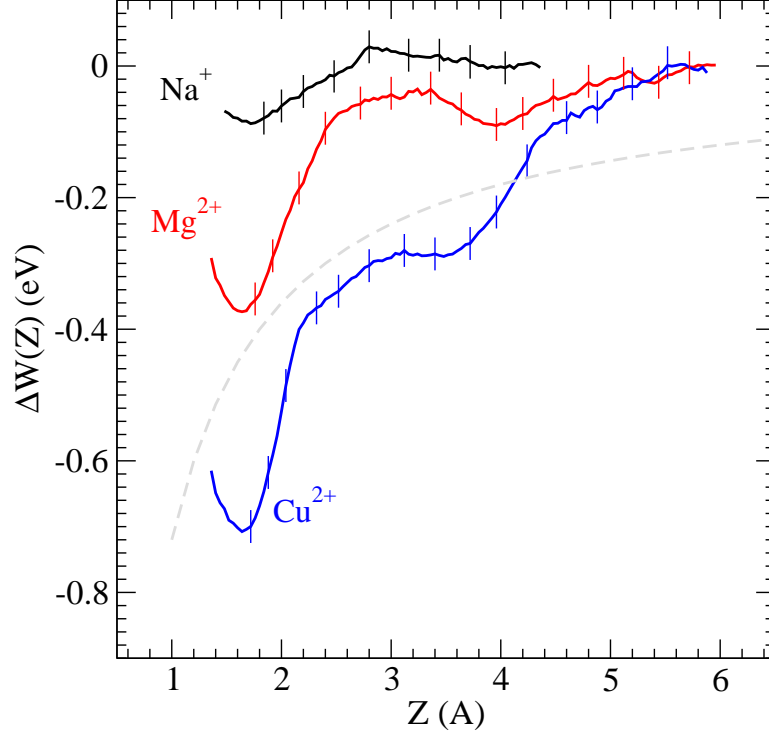


FIG. 1: Potential-of-mean-force (PMF) predictions of metal cation M^{n+} desorption profile ($\Delta W(Z)$) as a function of the vertical separation (Z) between M^{n+} and the O atom of the SiO^- group to which the cation is initially coordinated. Black, red, blue refer to $M=\text{Na}$, Mg , and Cu , respectively. Grey dashed line denotes the coulomb attraction between +2 and -2 charges screened by $\epsilon_o=78$. Vertical lines indicate the end points of sampling windows; they are not error bars.

as a cylinder with a radius $R=0.5 \text{ \AA}$ estimated from a completely unconstrained trajectory. Electrostatic corrections associated with image dipoles are added to Mg^{2+} PMF predictions. These corrections do not exceed 0.1 eV, are less than 0.03 eV for monovalent cations, and are further discussed in the S.I.

Figure 1 depicts the potentials-of-mean-force associated with Na^+ , Mg^{2+} , and Cu^{2+} desorption. The minima of $\Delta W(Z)$, relative to the asymptotic, large Z regime, are $-0.087 \pm 0.03 \text{ eV}$, $-0.38 \pm 0.05 \text{ eV}$, and -0.71 ± 0.07 , respectively. The uncertainties reflect one standard deviation.

First we focus on Na^+ on reconstructed β -cristobalite surface, with one deprotonated

SiOH group in the surface cell. In other words, 25% of the SiOH on one surface is deprotonated. Fig. 1 shows that the $\Delta W(Z)$ minimum is very shallow (-0.087 eV) for Na^+ . We start an AIMD trajectory with Na^+ coordinated to the surface site, without applying constraints. Na^+ remains there for ~ 45 ps; at longer times, it spontaneously escapes into the bulk solution. The statistics in Fig. 1 are collected prior to this spontaneous event. In subsequent sampling windows, PMF calculations circumvents this time scale problem by using constraining potentials. Substituting $\Delta W(Z)$ into Eq. 1, the free energy cost of Na^+ adsorbing on to this silica surface from a 1.0 M Na^+ solution is $\Delta G_{\text{abs}} = +0.13$ eV, if Na^+ is assumed to exhibit an activity coefficient of unity. The positive sign of ΔG_{abs} means there is no tendency for Na^+ to bind to the surface.

Fig. 2a-b depict configurations in trajectories constrained around $Z \sim 2.7$ Å and 3.0 Å, respectively. In both snapshots, the SiO^- group originally coordinated to Na^+ has become protonated. An H_2O molecule has spontaneously inserted between the SiOH group and the Na^+ before the second snapshot takes place. An apparent coordination number of four is seen in these snapshots only because the Na^+ is close to the surface. In the $Z \sim 4.2$ Å window, we have computed the pair correlation $g(r)$ between Na^+ and H_2O O atoms. The first minimum in the $g(r)$ is ~ 3.16 Å; integrating to this distance yields an average hydration number of 5.17. These values are similar to those computed for Na^+ in bulk water using AIMD⁴⁶ and polarizable force field⁴⁷ methods.

A recent calorimetry study reports favorable inner-sphere Na^+ adsorption enthalpy on partially deprotonated quartz particle surfaces at pH=4.¹⁶ Relating the quantitative enthalpic value per milligram silica sample to our calculations is challenging because the surface densities per type of deprotonated SiOH groups per unit surface area are not specified. Na^+ adsorption on silica has been inferred as inner-sphere¹⁶ or outer-sphere,¹⁰ depending on the measurement technique used, although the details of the silica samples and electrolytes differ. Our prediction that Na^+ is unbound on a specific model silica surface beyond a ~ 45 ps residence time may help interpret the data and resolve the discrepancy.

Recent AIMD simulations of deprotonated silica surfaces^{27,35} have reported persistent Na^+ coordination to the quartz (001) surface for the duration of trajectory lengths of ~ 10 ps. However, that surface exhibits a higher SiOH surface density than our model or amorphous silica. Na^+ can be also be bidentate or even tridentate on quartz (001). Future AIMD calculations to compute desorption PMF associated with Na^+ at bidentate sites will further

clarify transient inner- versus outer-sphere adsorption behavior.

We have also performed classical MD simulations using the same AIMD cristobalite surface, but increasing the surface area by a factor of four and adding a thicker aqueous layer (30 Å). Adsorption properties are obtained from unconstrained and umbrella sampling simulations. Final snapshots reveal that the Na^+ moves away from the SiO^- site and forms an inner-sphere monodentate complex with a neutral SiOH site. This is qualitatively similar to ReaxFF predictions.²³ Although the classical MD Na^+/SiO^- interactions have not yet been fitted to DFT/AIMD predictions and differ from AIMD simulations in the binding site configuration, the classical $\Delta W(Z)$ is qualitatively similar (Fig. S3 in the S.I.).

The first minimum in the Mg^{2+} $\Delta W(Z)$, at -0.37 eV, is located at ~ 1.68 Å (Fig. 1). A weak second minimum at 3.96 Å yields a -0.09 eV attraction, separated by a small barrier at 3.36 Å. This second valley represents an outer-sphere complex. In all configurations examined, Mg^{2+} is octahedrally coordinated to either 5 H_2O molecules and one SiO^- group (Fig. 2c) or 6 H_2O molecules (Fig. 2d). Integrating $\Delta W(Z)$ via Eq. 1 yields a favorable 0.14 eV binding free energy, unlike Na^+ which is predicted to be unbound. Calorimetry studies has shown that Mg^{2+} adsorption yields larger enthalpy release than Na^+ .¹⁶ Reference 8 has estimated a small 0.30 eV binding free energy between Mg^{2+} and silica surfaces, although it interprets the coordination as outer-sphere.

The grey dashed line depicts the coulombic attraction between ± 2 charges screened by $1/\epsilon_0$ appropriate to liquid water. The $\Delta W(Z)$ curve for Mg^{2+} does not exhibit such asymptotic behavior. Other classical force field-based PMF calculations with charged mineral surfaces and larger simulation cells than AIMD simulations also reach a plateau for $Z \sim 6$ Å; see Ref. 9 and Fig. S3 in this work. Hence the Mg^{2+} plateau in Fig. 1 does not appear related to finite size effects associated with AIMD simulation cells.

Fig. 1 also depicts the $\Delta W(Z)$ associated with Cu^{2+} . Substituting the relevant $\Delta W(Z)$ into Eq.1, the Cu^{2+} adsorption free energy is found to be a favorable -0.47 eV. This is substantially higher than our predicted Mg^{2+} value. It is a general trend that first row transition metal divalent cations tend to exhibit stronger binding behavior.⁵³ In the SiO^- - Cu^{2+} inner-sphere complex regime (Fig. 2e), Cu^{2+} is coordinated to 4 H_2O and a SiO^- group, which is slightly different from the 6-coordinated Mg^{2+} (Fig. 2d). Indeed, even in liquid water, it has been reported that the inner solvation shell of Cu^{2+} exhibits first hydration shell behaviors distinct from other first row transition metal ions.^{11,45}

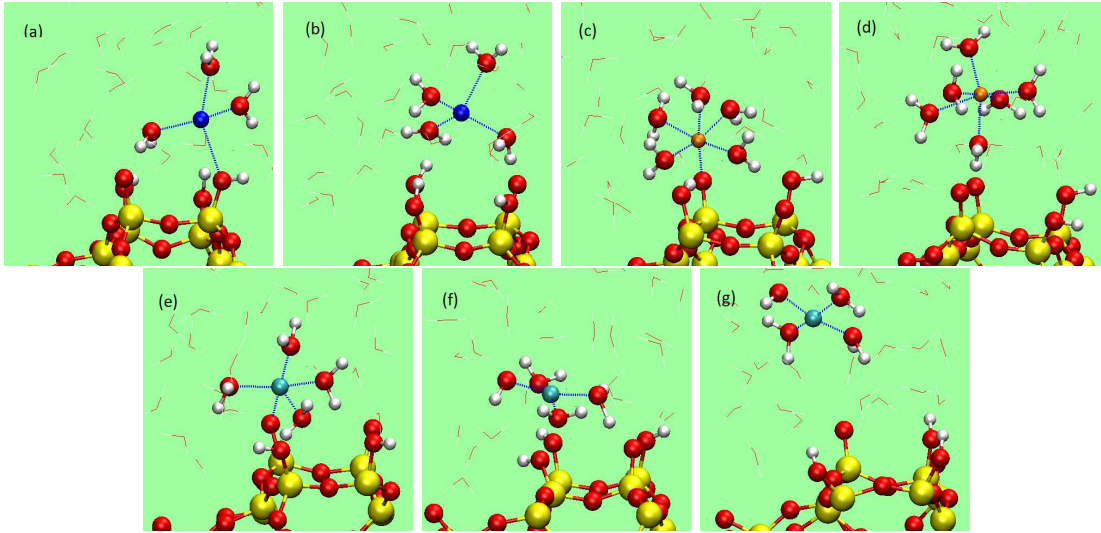


FIG. 2: Snapshots of (a)-(b) Na^+ , $Z \sim 2.7 \text{ \AA}$, and 3.0 \AA ; (c) Mg^{2+} , $Z \sim 1.6 \text{ \AA}$ (unconstrained in Z direction); (d) Mg^{2+} , $Z \sim 3.8 \text{ \AA}$; (e) Cu^{2+} , $Z \sim 1.6 \text{ \AA}$; (f) Cu^{2+} , $Z \sim 2.7 \text{ \AA}$; (g) Cu^{2+} , $Z \sim 4.5 \text{ \AA}$. Na, Mg, Cu, Si, O, and H atoms are colored in blue, orange, cyan, yellow, red, and white. H_2O are thin lines, except that those coordinated to the cation are depicted as ball-and-stick models. Thicker lines depict SiO-H bonds. No OH^- is coordinated to the cations in panels (a)-(e), but a OH^- clearly appears on Cu^{2+} in (f)-(g).

Away from the $Z > 2 \text{ \AA}$ regime, our AIMD simulations consistently predict that Cu^{2+} exists as a square-planar $\text{Cu}^{2+}(\text{OH}^-)(\text{H}_2\text{O})_3$ instead of an octahedral $\text{Cu}^{2+}(\text{H}_2\text{O})_6$ (Fig. 2f-g). The OH^- originates from an H_2O molecule directly coordinated to Cu^{2+} which has lost a H^+ to one of the two SiO^- groups initially on the surface when Z is small. This H_2O deprotonation event changes the Cu^{2+} coordination number drastically.

We have not applied AIMD to calculate the pK_a associated with H_2O molecules bonded to Cu^{2+} . But experimental pK_a of water in the $\text{M}^{2+}(\text{H}_2\text{O})_6$ first solvation shell have been quoted as 8 and 11.2-11.4 for Cu^{2+} and Mg^{2+} , respectively.^{50,51} Similar trends have been predicted in cluster-based DFT calculations.⁵² The silanol deprotonation pK_a for this reconstructed β -cristobalite surface has been predicted to be 7.0-8.1.³³ So the pK_a of SiOH and $\text{Cu}^{2+}(\text{H}_2\text{O})_6$ are very similar. The fact that the simulation cell contains a fraction of deprotonated SiOH means that the solution pH is pinned at the SiOH pK_a value. It is therefore reasonable that we observe deprotonation of $\text{Cu}^{2+}(\text{H}_2\text{O})_n$ but not of $\text{Mg}^{2+}(\text{H}_2\text{O})_6$. A lower pK_a in the first hydration shell has been linked to stronger tendency towards metal cation adsorption

or precipitation.¹⁴ Experimentally, SiOH pK_a has been proposed to follow bimodal⁴² or even trimodal⁴³ distributions. If Cu^{2+} is desorbed from a SiO^- group with $\text{pK}_a=4.5$,⁴² the $\text{Cu}^{2+}(\text{H}_2\text{O})_n$ complex would be insufficiently acidic to protonate the SiO^- group. So far, at atomic length-scale, such low pK_a SiOH groups have been identified only on quartz (0001) or amorphous silica surfaces,²⁶⁻²⁸ or as transient species.³³

In addition to the deprotonation of a H_2O coordinated to Cu^{2+} , AIMD simulations of all three cations involve proton exchange between neighboring SiO^- and SiOH groups on the same surface via water bridges once the cations are sufficiently far away from the surface. This will be further discussed below (Fig. 4).

In Fig. S3, classical force field MD simulations also yield a larger Cu^{2+} desorption free energy than Mg^{2+} . This is qualitatively consistent with AIMD results, although the magnitude of the inner-shell minimum in $\Delta W(Z)$ is overestimated compared to AIMD predictions, just as it is for Mg^{2+} . A separate simulation was performed with a hydroxide ion added to the Cu^{2+} system. The hydroxide ion remains in the first coordination shell of Cu^{2+} , but the Cu^{2+} coordination changes from 6-fold to 5-fold when the hydroxide ion is present. The $\Delta W(Z)$ for both ions are predicted to be qualitatively similar but with larger Cu^{2+} inner-shell solvation free energy. It cannot be ruled out that part of the overestimate lies in the inability of classical force field used to adequately describe cooperative acid-base behavior. Fine-tuning of the force field will be conducted in the future.

There are few AIMD simulations of Cu^{2+} on oxide surfaces, but predictions about other transition metal ions make useful comparisons. Ref. 37 applies AIMD simulations to show that removing Ni^{2+} from SiOH groups at clay edges requires a significant 0.69 eV to reach the first barrier at ~ 3 Å. This 0.69 eV free energy change is likely associated with an outer-sphere configuration rather than infinite separation between Ni^{2+} and the clay substrate. Cd^{2+} is predicted to exhibit a smaller, but still significant 0.23 eV initial barrier towards desorption.³⁶ Using classical force field-based molecular dynamics, Ref. 9 models Fe^{2+} desorption from both charge-neutral and deprotonated hematite (001) surfaces. While a quantitative comparison with our charged surface should not be made, the PMF reported there for the neutral surface has less structure in $\Delta W(z)$ beyond $z = 4$ Å than in the Mg^{2+} PMF in Ref. 18 regardless of the force field used. The charged surface with a $(\text{SiO}^-)_2\text{Fe}(\text{II})$ binding site exhibits ~ 1.7 - 2.2 eV first minima in $\Delta W(Z)$. We stress that none of the calculations discussed for this comparison purpose have reported cooperative acid-base reactions

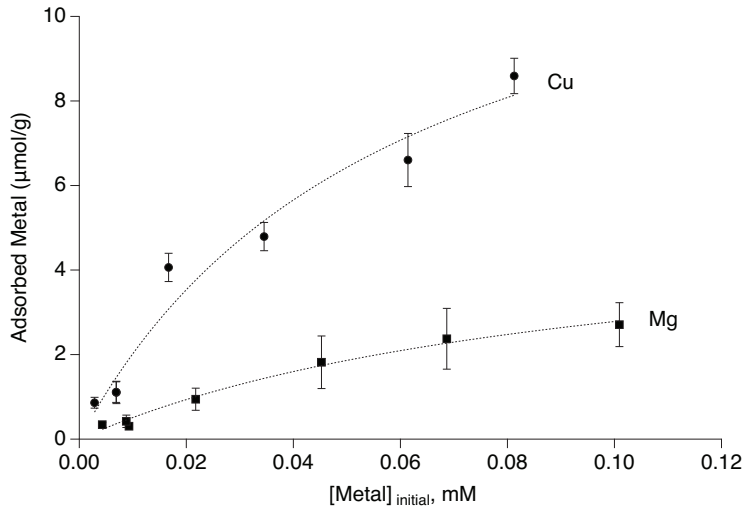


FIG. 3: Competitive batch adsorption measurements showing that Cu^{2+} adsorbs more readily than Mg^{2+} on fumed silica surfaces at different electrolyte concentrations.

– either because they apply classical force fields or because the material surface is different.

On amorphous silica surfaces, Cu^{2+} can form dimers.¹² At sufficiently high pH it precipitates to form $\text{Cu}(\text{OH})_2$. Our AIMD simulation cells, which contain one divalent cation, cannot model dimerization and precipitation. However, the intriguing desorption configurations we predict are likely precursors to such complex Cu^{2+} behavior if more than one Cu^{2+} is present.

Batch adsorption isotherm experiments were performed to evaluate the competitive adsorption of Cu and Mg on fumed silica and provide validation of DFT calculations. For competitive adsorption studies, $\text{Cu}(\text{NO}_3)_2$ and $\text{Mg}(\text{NO}_3)_2$ were added to each 50 mL centrifuge tube with concentrations ranging from 0.005 mM to 0.1 mM and brought up to 10 mL total volume with Milli-Q water. The pH was adjusted to 6.0 ± 0.1 using dilute HNO_3 or NH_4OH .

Experimental data was fit to the Langmuir adsorption model, which represents homogeneous adsorption and estimates the adsorption maximum by limiting adsorption to monolayer coverage. The Langmuir adsorption equation applied for analysis is shown in Eq. 2,^{48,49}

$$q_e = \frac{K_L q_m [\text{M}^{n+}]_{\text{eq}}}{1 + K_L [\text{M}^{n+}]_{\text{eq}}} \quad (2)$$

where q_e is the mass normalized equilibrium adsorption of the metal for Mg^{2+} and Cu^{2+} ($\mu\text{mol/g}$), q_m is the mass normalized adsorption values for these cations ($\mu\text{mol/g}$), and K_L

is the Langmuir constant ($L/\mu\text{mol}$), The Langmuir fitting parameters were estimated by fitting the data using the curve fitting function in Igor Pro. Other experimental details are given in the S.I.

The experimental results are summarized in Fig. 3 depicting the results of competitive adsorption of Cu^{2+} and Mg^{2+} on fumed silica surfaces. The background electrolyte was 0.01 M NH_4NO_3 at $\text{pH}=6.5$. Cu has a higher affinity towards silica surface compared to Mg. The adsorption isotherm data is fit with the Langmuir adsorption model in which the adsorption maximum values, q_m , are $14\pm 3 \mu\text{mol/g}$ and $5\pm 1 \mu\text{mol/g}$, for Cu^{2+} and Mg^{2+} , respectively. Likewise, the distribution factors and the resulting separation factor of Cu^{2+} over Mg^{2+} maintained values of 4-5 over a large concentration (see the S.I.). Although the experimental surface termination is likely different from the reconstructed β -cristobalite (001) model used in our AIMD studies, the measurements and modeling consistently show that Cu^{2+} is more strongly bound. A quantitative comparison is currently impossible because AIMD simulations contain only one Cu^{2+} that cannot form dimers.

Next we address the static distributions in the protonation state of the SiOH surface group coordinated to the cation as desorption proceeds. Nearest-neighbor SiOH groups are $\sim 5 \text{ \AA}$ apart, and H^+ exchanges occur via water bridges. For Na^+ (Fig. 4a), in sampling windows centered around $Z\sim 2.7 \text{ \AA}$ and below, the silanol group is deprotonated at the cation binding site. This maximizes electrostatic attraction with Na^+ . The exception is $Z\sim 1.9 \text{ \AA}$. A closer examination reveals that the Na^+ ion is vacillating between two SiO^-/SiOH groups, coordinating to one and then the other. When Z is around ~ 3.0 to 4.0 \AA , $P(Z)$ fluctuates between 0.4 and 1.0. Asymptotically, when Na^+ is infinitely far away, each of the four SiOH on this surface should have an equal, 25% probability of being deprotonated. The AIMD trajectories are not sufficiently long to reflect that. We stress that our trajectory lengths are chosen to converge $\Delta W(Z)$ to a certain precision, not necessarily other properties like mean protonation states.

Mg^{2+} and Cu^{2+} exhibit qualitatively similar protonation behavior (Fig. 4b,c), despite the fact that their $\Delta W(Z)$ are significantly different; Cu^{2+} dissociates a H_2O at large Z while Mg^{2+} does not; and the error bars in $P(Z)$ may be large. $P(Z)\approx 0$ at $Z<2.4 \text{ \AA}$ presumably because M^{2+} strongly repels the like-charged H^+ in its vicinity. $P(Z)\sim 1$ from 2.4 to 3.3 \AA the region between inner- and outer-sphere complexes. It drops to a low value around 3.6 \AA , then returns to higher average protonated states. For both Mg^{2+} and Cu^{2+} , $P(Z)$

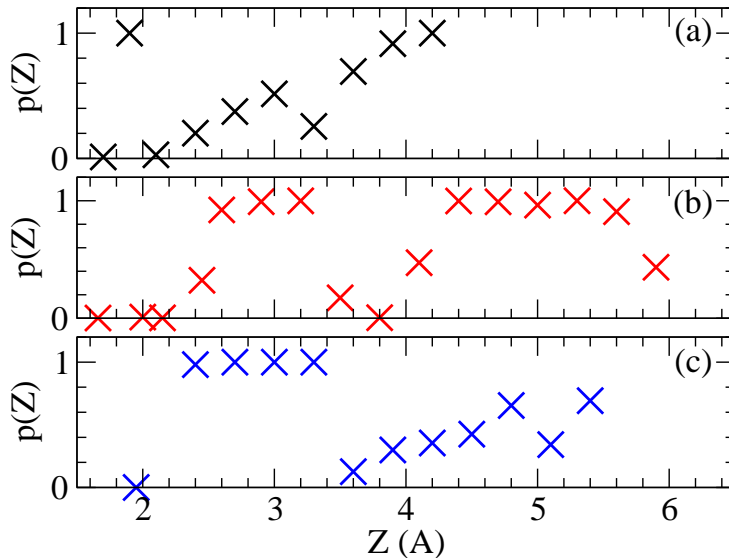


FIG. 4: Protonation states ($p(Z)$) of SiO^- group originally bonded to M^{n+} , as a function of sampling window Z . (a) Na^+ ; (b) Mg^{2+} ; (c) Cu^{2+} . The SiO^- is “protonated” if its O^- ion is within 1.25 \AA of any proton in the simulation cell.

varies non-monotonically as the cation desorbs. This may be a useful consideration when defining the SiOH protonation as a “slow variable” in future metadynamics ion desorption calculations.

The SI considers dynamic correlations between SiOH protonation states and $\Delta W(Z)$. We conclude that SiOH protonation state fluctuations are not strongly dynamically correlated with cation desorption free energies in windows where $0 < P(Z) < 1$. This suggests that AIMD PMF predictions are reliable despite the somewhat slow $p(t)$ fluctuation time scales.

In conclusion, we have used *ab initio* molecular dynamics potential-of-mean-force techniques to calculate the desorption free energies of Na^+ , Mg^{2+} , and Cu^{2+} from a model silica surface with a $4.0/\text{nm}^2$ SiOH surface density and $\text{pK}_a \sim 7.0\text{-}8.1$. The cations are initially adsorbed in an inner-sphere monodentate manner. Na^+ at standard state (1.0 M concentration) is predicted to be unbound, while the divalent cations are predicted to be thermodynamically stable when coordinated to SiO^- groups by 0.14 and 0.47 eV, respectively, in inner-sphere configurations. The predicted trends are in qualitative agreement with competitive batch adsorption measurements. We argue that negatively charged surfaces which allow bi- or tri-dentate SiO^- binding to metal ions should favor inner-sphere

adsorption over outer-sphere adsorption even more strongly. Water-bridge-assisted proton exchange between surface SiOH groups is observed as cation desorption proceeds, which increases interfacial fluctuations. The protonation state ($P(Z)$) of the SiO^- group at the binding site is not a monotonic function of the separation Z between the cation and the surface. A water molecular coordinated to Cu^{2+} donates a proton to surface SiO^- with predicted pK_a of about 7.0-8.1,³³ forming 4-coordinated $\text{Cu}^{2+}(\text{OH}^-)(\text{H}_2\text{O})_3$ complexes. To within computational accuracy, this is consistent with the experimental $\text{Cu}^{2+}(\text{H}_2\text{O})_6$ pK_a of about 8. In contrast, Mg^{2+} invariably forms octahedral $\text{Mg}^{2+}(\text{H}_2\text{O})_6$ or $\text{Mg}^{2+}(\text{H}_2\text{O})_5(\text{SiO}^-)$ complexes. Our conclusion that the $\text{Cu}^{2+}\text{OH}^-$ complexes occur as Cu^{2+} desorbs also informs speciation choices for future classical-MD investigations. While AIMD is computationally costly, our predictions will be useful for benchmarking and assessing the applicability of simpler molecular force fields for ion-binding application, and paves the way for enumerating desorption free energies from multiple binding sites in the future.

Supporting Information Available: Details of PMF calculations; snapshots of cation adsorption on silica surfaces and classical PMF results conducted using classical force field-based molecular dynamics; details of batch adsorption measurements; dynamical correlations between SiOH protonation state and cation desorption

We thank Jessica Rimsza and Jacob Harvey for useful discussions. Sandia National Laboratories is a multimission laboratory managed and operated by National Technology and Engineering Solutions of Sandia, LLC, a wholly owned subsidiary of Honeywell International, Inc., for the U.S. Department of Energys National Nuclear Security Administration under contract de-na0003525. This work is based on materials support by the U.S. DOE Office of Basic Energy Sciences, Division of Chemical Sciences, Geosciences, and Biosciences.

¹ DeWalt-Kerian, E.L.; Kim, S. Azam, M.S.; Zeng, H.; Liu, Q.; Gibbs, J.M. pH-dependent Inversion of Hofmeister Trends in the Water Structure of the Electric Double Layer. *J. Phys. Chem. Lett.* **2017**, *8*, 2855-2861.

² Shen, Z.; Kerisit, S.N.; Stack, A.G.; Rosso, K.M. Free-energy Landscape of the Dissolution of Gibbsite at High pH. *J. Phys. Chem. Lett.* **2018**, *9*, 1809-1814.

³ Peng, Q.M.; Guo, J.X.; Zhang, Q.R.; Xiang, J.Y.; Liu, B.Z.; Zhou, A.G.; Liu, R.P.; Tian, Y.T.

- Unique Lead Adsorption Behavior of Activated Hydroxyl Group in Two-Dimensional Titanium Carbide. *J. Am. Chem. Soc.* **2014**, *136*, 4113-4116.
- ⁴ Hayes, K.F.; Roe, A.L.; Brown, G.E.; Hodgson, K.O., Leckie, J.O.; Parks, G.A. In Situ X-Ray Adsorption Study of Surface Complexes – Selenium Oxyanions on α -FeOOH. *Science* **1987**, *238*, 783-786.
- ⁵ Nihonyanagi, S.; Yamaguchi, S.; Tahara, T. Counterion Effect on Interfacial Water at Charged Interfaces and its Relevance to the Hofmeister Series. *J. Am. Chem. Soc.* **2014**, *136*, 6155-6158.
- ⁶ Sverjensky, D.A. Prediction of the Speciation of Alkaline Earths Adsorbed on Mineral Surfaces in Salt Solutions. *Geochim. Cosmochim. Acta* **2006**, *70*, 2427-2453.
- ⁷ Leung, K.; Criscenti, L.J. Lead and Selenite Adsorption at Water-Goethite Interfaces from First Principles. *J. Phys. Condens. Matter* **2017**, *29*, 365101, and references therein.
- ⁸ Hayes, P.L.; Malin, J.N.; Jordan, D.S.; Geiger, F.M. Get charged up: Nonlinear Optical Voltammetry for Quantifying the Thermodynamics and Electrostatics of Metal Cations at Aqueous/Oxide Interfaces. *Chem. Phys. Lett.* **2010**, *499*, 183-192.
- ⁹ Kerisit, S.; Zarzycki, P.; Rosso, K.M. Computational Molecular Simulation of the Oxidative Adsorption of Ferrous Iron at the Hematite (001)-Water Interface. *J. Phys. Chem. C* **2015**, *119*, 9242-9252.
- ¹⁰ Kim, Y.; Kirkpatrick, R.J. ²³Na and ¹³³Cs NMR Study of Cation Adsorption on Mineral Surfaces: Local Environments, Dynamics, and Effects of Mixed Cations. *Geochim. Cosmochim. Acta* **1997**, *61*, 5199-5208.
- ¹¹ Cheah, S.-F.; Brown, G.E.; Parks, G.A. XAFS Study of Cu Model Compounds and Cu²⁺ Sorption Products on Amorphous SiO₂, γ -Al₂O₃, and Anatase. *Amer. Mineral.* **2000**, *85*, 118-132.
- ¹² Cheah, S.F.; Brown, G.E. Jr.; Parks, G.A. XAFS Spectroscopy Study of Cu(II) Sorption on Amorphous SiO₂ and γ -Al₂O₃: Effects of Substrate and Time on Sorption Complexes. *J. Coll. Interface Sci.* **1998**, *208*, 110-128.
- ¹³ Cheah, S.F.; Brown, G.E. Jr.; Parks, G.A. The Effect of Substrate Type and 2,2'-Bipyridine on the Sorption of Copper(II) on Silica and Alumina. Voigt, J.A., Wood, T.E., Bunker, B.C., Casey, W.H., Crossey, L.J. (Eds.), *Mater. Res. Soc. Proc.* **1997**, *432*, 231-236.
- ¹⁴ Elliot, H.A., Liberati, M.R.; Huang, C.P. Competitive Adsorption of Heavy Metals by Soils. *J. Envir. Quality* **1986**, *15*, 214-219.

- ¹⁵ Subramaniam, K.; Vithayaveroj, V.; Yiacoymi, S.; Tsouris, C. Copper Uptake by Silica and Iron Oxide under High Surface Coverage Conditions: Surface Charge and Sorption Equilibrium Modeling. *J. Coll. Interface Sci.* **2003**, *268*, 12-22.
- ¹⁶ Allen, M.; Machesky, M.L.; Wesolowski, D.J.; Kabengi, N. Calorimetric Study of Alkali and Alkaline-Earth Cation Adsorption and Exchange at the Quartz-Solution Interface. *J. Coll. Interface Sci.* **2017**, *504*, 538-548.
- ¹⁷ Hocine, S.; Hartkamp, R.; Siboulet, B.; Duvail, M.; Coasne, B.; Turq, P.; Dufreche, J.-F. How Ion Condensation Occurs at a Charged Surface: a Molecular Dynamics Investigation of the Stern layer for Water-Silica Interfaces. *J. Phys. Chem. C* **2016**, *120*, 963-973.
- ¹⁸ Katz, L.E.; Criscenti, L.J.; Chen, C.-C.; Larentzos, J.P.; Liljestrand, H.M. Temperature Effects on Alkaline Earth Metal Ions Adsorption on Gibbsite: Approaches from Macroscopic Sorption Experiments and Molecular Dynamics Simulations. *J. Coll. Interface Sci.* **2013**, *399*, 68-76.
- ¹⁹ Hartkamp, R.; Siboulet, B.; Dufreche, J.F.; Coasne, B. Ion-Specific Adsorption and Electroosmosis in Charged Amorphous Porous Silica. *Phys. Chem. Chem. Phys.* **2015**, *17*, 24683-24695.
- ²⁰ Loganathan, N.; Kalinichev, A.G. Quantifying the Mechanisms of Site-Specific Ion Exchange at an Inhomogeneously Charged Surface: Case of Cs⁺/K⁺ on Hydrated Muscovite Mica. *J. Phys. Chem. C* **2017**, *121*, 7829-7836.
- ²¹ Fogarty, J.C.; Aktulga, H.M.; Grama, A.Y.; Van Duin, A.C.; Pandit, S.A. A Reactive Molecular Dynamics Simulation of the Silica-Water Interface. *J. Chem. Phys.* **2010**, *132*, 174704.
- ²² Mahadevan, T.S.; Garofalini, S.H. Dissociative Water Potential for Molecular Dynamics Simulations. *J. Phys. Chem. B* **2007**, *111*, 8919-8927.
- ²³ Rimsza, J.M.; Jones, R.E.; Criscenti, L.J. Interaction of NaOH Solutions with Silica Surfaces. *J. Coll. Interface. Sci.* **2018**, *516*, 128-137.
- ²⁴ Liu, X.; Cheng, J.; Sprik M.; Lu, X.C.; Wang, R. Understanding Surface Acidity of Gibbsite with First Principles Molecular Dynamics Simulations. *Geochim. Cosmochim. Acta*, **2013**, *120*, 487-495.
- ²⁵ Churakov, S.V.; Labbez, C.; Pegado, L.; Sulpizi, M. Intrinsic acidity of Surface Sites in Calcium Silicate Hydrates and its Implication to their Electrokinetic Properties. *J. Phys. Chem. C* **2014**, *118*, 11752-11762.
- ²⁶ Pfeiffer-Laplaud, M.; Gageot, M.-P.; Sulpizi, M. pK(a) at Quartz/Electrolyte Interfaces. *J. Phys Chem. Lett.* **2016**, *7*, 3229-3234.

- ²⁷ Pfeiffer-Laplaud M.; Gaigeot, M.-P. Electrolytes at the Hydroxylated (0001) α -Quartz/Water Interface: Location and Structural Effects on Interfacial Silanols by DFT-based MD. *J. Phys Chem. C* **2016**, *120*, 14034-14047.
- ²⁸ Pfeiffer-Laplaud, M.; Gaigeot, M.-P. Adsorption of Singly Charged Ions at the Hydroxylated (0001) α -Quartz/Water Interface. *J. Phys Chem. C* **2016**, *120*, 4866-4880.
- ²⁹ Pfeiffer-Laplaud, M.; Costa, D.; Tielens, F.; Gaigeot, M.-P.; Sulpizi, M. Bimodal Acidity at the Amorphous Silica/Water Interface. *J. Phys Chem. C* **2015**, *119*, 27354-27362.
- ³⁰ Tazi, S.; Rotenberg, B.; Salanne, M.; Sprik, M.; Sulpizi, M. Absolute Acidity of Clay Edge Sites from Ab-Initio Simulations. *Geochim. Cosmochim. Acta* **2012**, *94*, 1-11.
- ³¹ Sulpizi, M.; Gaigeot, M.-P.; Sprik, M. The Silica-Water Interface: How the Silanols Determine the Surface Acidity and Modulate the Water Properties. *J. Chem. Theor. Comput.* **2012**, *8*, 1037-1047.
- ³² Cheng, J.; Sulpizi, M.; Sprik, M. Redox Potentials and pK(a) for Benzoquinone from Density Functional Theory Based Molecular Dynamics. *J. Chem. Phys.* *2009*, *131*, 154504.
- ³³ Leung, K.; Nielsen, I.M.B.; Criscenti, L.J. Elucidating the Bimodal Acid-Base Behavior of the Water-Silica Interface from First Principles. *J. Am. Chem. Soc.*, **2009**, *131*, 18358-18365.
- ³⁴ Leung, K.; Criscenti, L.J. Predicting the Acidity Constant of a Goethite Hydroxyl Group From First Principles. *J. Phys. Condens. Matter* **2012**, *24*, 124015.
- ³⁵ Dellostritto, M.J.; Kubicki, J.D.; Sofo, J.O. Effect of Ions on H-Bond Structure and Dynamics at the Quartz(101)-Water Interface. *Langmuir*, **2016**, *32*, 11353-11365.
- ³⁶ Zhang, C.; Liu, X.; Lu, X.; Meijer, E.J.; Wang, K.; He, M.; Wang, R. Cadmium(II) Complexes Adsorbed on Clay Edge Surfaces: Insight from First Principles Molecular Dynamics Simulations. *Clays and Clay Minerals*, **2016**, *64*, 337-347.
- ³⁷ Zhang, C.; Liu, X.; Lu, X.; He, M.; Meijer, E.J.; Wang, R. Surface Complexation of Heavy Metal Cations on Clay Edges: Insights from First Principles Molecular Dynamics Simulation of Ni(II). *Geochim. Cosmochim. Acta* **2017**, *203*, 54-68.
- ³⁸ Brinker, C.J.; Scherer, G.W. *Sol-Gel Science*; Academic Press, London, 1990, Ch. 10.
- ³⁹ Perdew, J.P.; Burke, K.; Ernzerhof, M. Generalized Gradient Approximation Made Simple. *Phys. Rev. Lett.* **1996**, *77*, 3865-3868.
- ⁴⁰ Kresse, G.; Joubert, J. From ultrasoft pseudopotentials to the projector augmented-wave method. *Phys. Rev. B* **1999**, *59*, 1758-1775.

- ⁴¹ Kresse, G.; Furthmüller, J. Efficient Iterative Schemes for Ab Initio Total-Energy Calculations Using a Plane-Wave Basis Set. *Phys. Rev. B* **1996**, *54*, 11169.
- ⁴² Shen Y.R.; Ostroverkhov, V. Sum-Frequency Vibrational Spectroscopy on Water Interfaces: Polar Orientation of Water Molecules at Interfaces. *Chem. Rev.* **2006**, *106*, 1140-1154.
- ⁴³ Darlington, A.M.; Gibbs-Davis, J. Bimodal or Trimodal? The Influence of Starting pH on Site Identity and Distribution at the Low Salt Aqueous/Silica Interface. *J. Phys. Chem. C* **2015**, *119*, 16560-16567.
- ⁴⁴ Blumberger, J.; Klein, M.L. Revisiting the Free Energy Profile for the Nucleophilic Attack of Hydroxide on Formamide in Aqueous Solution. *Chem. Phys. Lett.* **2006**, *422*, 210-217.
- ⁴⁵ Pasquarello, A.; Petri, I.; Salmon, P.S.; Parisel, O.; Car, R.; Toth, E.; Powell, D.H.; Fischer, H.E.; Helm, L.; Merbach, A.E. First Solvation Shell of the Cu(II) Aqua Ion: Evidence for Fivefold Coordination. *Science*, **2001**, *291*, 856-859.
- ⁴⁶ Rowley, C.N.; Roux, B. The Solvation Structure of Na⁺ and K⁺ in Liquid Water Determined from High Level *ab initio* Molecular Dynamics Simulations. *J. Chem. Theory Comput.* **2012**, *8*, 3526-3535.
- ⁴⁷ Grossfield, A.; Ren, P.; Ponder, J.W. Ion Solvation Thermodynamics from Simulation with a Polarizable Force Field. *J. Am. Chem. Soc.* **2003**, *125*, 15671-15682.
- ⁴⁸ Langmuir, I. The Adsorption of Gases on Plane Surfaces of Glass, Mica and Platinum. *J. Am. Chem. Soc.* **1918**, *40*, 1361-1403.
- ⁴⁹ Mahmoud, M.A. Kinetics and Thermodynamics of Aluminum Oxide Nanopowder Adsorbent for Fe(III) from Aqueous Solutions. *Beni-Suef Univ. J. Basic Applied Sci.* **2015**, *4*, 142-149.
- ⁵⁰ Stumm, W.; Morgan, J.J. *Aquatic Chemistry: Chemical Equilibria and Rates in Natural Waters*, 3rd ed.; John Wiley & Sons: New York, 1996.
- ⁵¹ Baes, C.F.; Mesmer, R.E. *Hydrolysis of Cations*, Krieger Publishing Company: Malabar, FL, 1976.
- ⁵² Jackson, V.E.; Felmy, A.R.; Dixon, D.A. Prediction of the pK_a's of Aqueous Metal Ion +2 Complexes. *J. Phys. Chem. A* **2015**, *119*, 2926-2939.
- ⁵³ Langmuir, D. *Aqueous Environmental Geochemistry* **1997** (Prentice, New Jersey)

